Yang, X., **Jomaa, S.**, **Büttner, O.**, **Rode, M.** (2019):
Autotrophic nitrate uptake in river networks: A modeling approach using continuous high-frequency data
Water Res. **157** , 258 - 268

http://dx.doi.org/10.1016/j.watres.2019.02.059

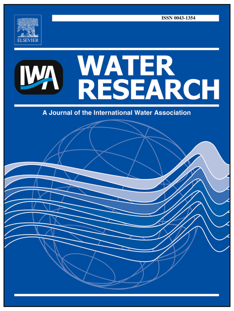

Autotrophic nitrate uptake in river networks: A modeling approach using continuous high-frequency data

Xiaoqiang Yang, Seifeddine Jomaa, Olaf Büttner, Michael Rode

PII: S0043-1354(19)30275-1
DOI: https://doi.org/10.1016/j.watres.2019.02.059
Reference: WR 14540

To appear in: *Water Research*

Received Date: 2 November 2018
Revised Date: 25 February 2019
Accepted Date: 26 February 2019

Please cite this article as: Yang, X., Jomaa, S., Büttner, O., Rode, M., Autotrophic nitrate uptake in river networks: A modeling approach using continuous high-frequency data, *Water Research*, https://doi.org/10.1016/j.watres.2019.02.059.

Reach-scale nitrate uptake

Open-canopy stream

Deciduous shaded stream

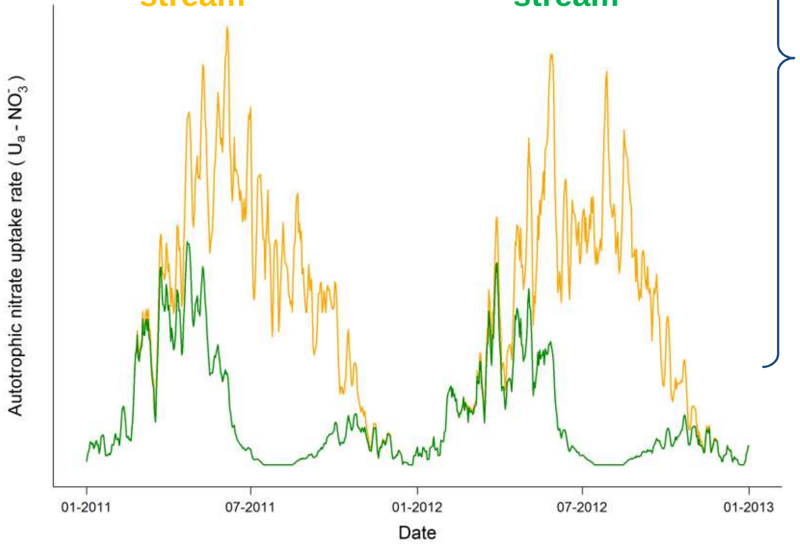

The catchment model (mHM-Nitrate)

Upscaling

Network-scale modeling

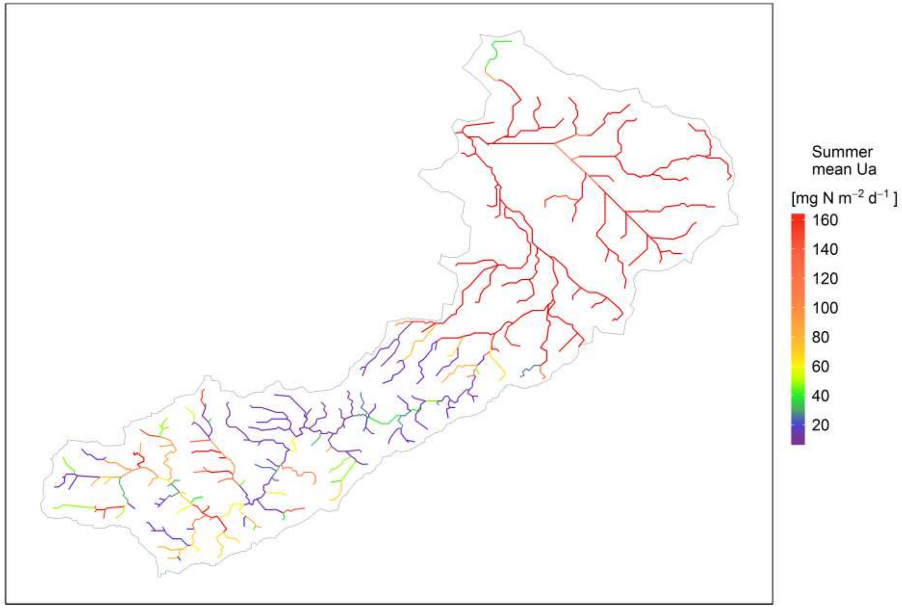

Autotrophic nitrate uptake in river networks: A modeling approach using continuous high-frequency data

Xiaoqiang Yang, Seifeddine Jomaa, Olaf Büttner and Michael Rode

Department of Aquatic Ecosystem Analysis and Management, Helmholtz Centre for Environmental Research – UFZ, Brückstrasße 3a, 39114 Magdeburg, Germany

Corresponding author: X. Yang (xiaoqiang.yang@ufz.de)

Abstract

High-frequency sensor measurements enable calculation of continuous autotrophic nitrate uptake rate based on its intrinsic relationship with gross primary production (GPP). The spatiotemporally available data offer prospects to advance process understandings across scales. We used continuous 15-min data (2011-2015) from a forest upstream reach and an agricultural downstream reach of the Selke River, Germany. Based on the high-frequency data, we developed a parsimonious approach for regionalizing the autotrophic uptake rate, considering effects of global radiation and riparian shading. For networked modeling, we integrated this approach into the fully distributed mesoscale hydrological nitrate model (mHM-Nitrate). Daily GPP-based uptake rate calculations showed distinct seasonal patterns and ranges in the agricultural and forest streams (mean values were 80.9 and 15.5 $mg\ N\ m^{-2} d^{-1}$, respectively). Validation in the two streams showed acceptable performance (R^2 = 0.47and 0.45, respectively) and spatial transferability of the regionalization approach, given its parsimony. Networked modeling results showed high spatiotemporal variability in nitrate transport and uptake throughout the river network. The magnitude of gross uptake increased, whereas uptake efficiency decreased significantly along stream order. Longitudinal analysis in the main stem of the Selke River revealed that riparian shading and inter-annual hydrochemical variations strongly influenced daily dynamics of the uptake efficiency. This study provides a parsimonious and transferable procedure for regionalizing in-stream autotrophic nitrate uptake based on high-frequency data at reach scale. Integrating this approach in the mHM-Nitrate model allows detailed nitrate transport and in-stream uptake processes to be investigated throughout river networks.

Key words: high-frequency monitoring; water quality; stream metabolism; regionalization; network upscaling; the fully distributed mHM-Nitrate model.

1. Introduction

Streams deliver nutrients to catchment outlets and estuaries, and also transform and remove nutrients as traveling through the river network (Alexander et al. 2009). Hydrological, morphological and biogeochemical characteristics influence in-stream nutrient processing greatly, resulting in high spatiotemporal variability throughout the river network (Bernhardt et al. 2005). The in-stream processing is also influenced by factors resulting from terrestrial processes, such as nutrient availability and hydrological conditions (Mulholland et al. 2008). With such a high level of complexity, investigating nutrient dynamics at the river network scale remains challenging (Helton et al. 2011).

Following the nutrient spiraling concept (i.e., the cycling of nutrient being assimilated, temporarily retained and mineralized (Ensign and Doyle 2006)), reach-scale studies have provided much information on influential factors and in-stream uptake quantifications (Mulholland et al. 2008). Due to experimental constraints, traditional tracer studies are mostly conducted in headwater streams rather than in large streams and rivers. Networked nutrient spiraling metrics (e.g., uptake rate constant k) have been correlated with influential factors (e.g., water depth or nutrient concentrations) (Mulholland et al. 2008, Ye et al. 2017) using empirical functions. Selections of these functions (e.g., first-order kinetics) and their corresponding parameters are based on measurements across experimental sites/reaches (Alexander et al. 2009, Helton et al.

2011). However, the limitations of regionalizing and upscaling procedures are reflected in (1) dubious representativeness of measurements in small headwater streams for large streams with diverse natural characteristics and anthropogenic impacts, (2) inadequate quantification of distal factors (Helton et al. 2011), e.g., riparian vegetation and land cover conditions that influence stream light availability, and (3) insufficient coverage of spatiotemporal variations in in-stream processes and terrestrial allochthonous inputs.

Nitrate (NO_3^-) has been intensively investigated due to its mobility and environmental impacts (Grant et al. 2018). The in-stream fate of $NO_3^-$is strongly correlated with ecosystem metabolism in lotic systems due to biotic demand in benthic biofilms and hyporheic zones (Bernhardt et al. 2018, Gomez-Velez et al. 2015, Rode et al. 2016a). Measurements in small headwaters demonstrate a strong relationship between total NO_3^- uptake and ecosystem metabolism rates, and a significant linear regression between NO_3^- diel amplitude (due to autotrophic uptake) and gross primary production (GPP) (Roberts and Mulholland 2007). However, traditional sampling campaigns are mostly conducted in streams where and when stream conditions are optimum (Bernhardt et al. 2018). Consequently, they are not sufficient for estimating temporal dynamics (Heffernan and Cohen 2010), nor for transferal to different stream conditions.

The development of sensor techniques allows continuous monitoring under a much wider range of stream conditions and therefore improves understanding of ecosystem processes (Rode et al. 2016b). Among others, NO_3^- sensors are widely available and the autotrophic NO_3^- uptake rate ($U_{a-NO_3^-}, mg\ N\ m^{-2}\ d^{-1}$) can be measured directly from high-frequency NO_3^- concentration measurements, i.e., the diel amplitude. Based on high-frequency monitoring, Heffernan and Cohen (2010) found a strong correlation between measured $U_{a-NO_3^-}$ and calculations based on measured GPP and the stoichiometric ratio in a subtropical spring-fed river in the USA. Rode et al. (2016a) related measured $U_{a-NO_3^-}$ to GPP based on high-frequency data in forest and agricultural streams in Germany, and demonstrated the agreement between regression and stoichiometric methods. Therefore, high-frequency monitoring facilitates reliable in-stream measurements, which can stimulate new insights into NO_3^- uptake processing across stream conditions.

Given abundant NO_3^- availability, stream metabolism is usually controlled by physical factors, such as light, temperature and flow disturbance (O'Connor et al. 2012, Uehlinger 2006). Among proximal factors, light (i.e., photosynthetically active radiation - PAR) dominates the variation in GPP (Mulholland et al. 2001, Roberts et al. 2007). Meanwhile, distal factors (e.g., land cover and riparian vegetation) largely impact the stream surface light availability (Bernot et al. 2010). However, the surface light regime and its impact on GPP have not been quantified adequately, most likely due to the difficulty in relating the light regimes to widely available data (Bernhardt et al. 2018). Based on continuous high-frequency sensor deployment, Rode et al. (2016a) explicitly showed different seasonal patterns of GPP in closed- and open-canopy streams. Interestingly, the patterns are highly consistent with those of PAR measured above forested stream surface and above forest canopy, respectively (measurements in Roberts et al. (2007)). Therefore, information derived from continuous high-frequency monitoring can be used for relating in-stream autotrophic NO_3^- uptake to its driving factors, especially under diverse light regimes.

One main challenge in modeling networked NO_3^- uptake, especially uptake efficiency (i.e., the percentage of the uptake amount to the load), is covering the spatiotemporal heterogeneity of terrestrial exports (e.g., NO_3^- load). Most network models emphasize in-stream processes and simplify greatly representations of terrestrial processes. They either statistically relate terrestrial exports to catchment characteristics (e.g., the SPARROW model) (Wollheim et al. 2008) or define one or more flow components as end-members. Those simplifications restrict the ability to model river networks that have heterogeneous conditions, and in which allochthonous terrestrial inputs are likely more diverse (Dupas et al. 2017). Alternatively, mechanistic catchment water quality models describe catchment characteristics thoroughly (Rode et al. 2010); Among them, grid-based models are preferable due to their inherent higher degree of spatial representation (Yang et al. 2018). Moreover, the grid-based routing structure provides detailed reach-scale information (e.g., stream geomorphological features) for analyzing in-stream processes. To our knowledge, mechanistic catchment models that provide detailed terrestrial exports have rarely been used to upscale reach-scale advances to the network scale.

In this study, we propose a parsimonious regionalization approach for $U_{a-NO_3^-}$ based on continuous high-frequency NO_3^- concentration and stream metabolic data (2011-2015) in a forest and an agricultural stream reach of the Selke River, Germany. We upscale the findings to the river network scale based on the fully distributed catchment NO_3^- model (mHM-Nitrate) (Yang et al. 2018). Influential factors of global radiation (GR) and riparian shading are chosen to quantify the stream surface light availability. The new data and the modeling approach allow us to (1) obtain continuous daily $U_{a-NO_3^-}$ data from the high-frequency measurements and the intrinsic relationship between $U_{a-NO_3^-}$ and GPP, (2) validate the performance of the $U_{a-NO_3^-}$ regionalization approach and test the spatial transferability for deviating stream riparian conditions, and (3) upscale the approach to the whole Selke river network based on the mHM-Nitrate model and provide detailed spatiotemporal information on NO_3^- transport and uptake at the river network scale.

2. Materials and Methods

2.1. Study site and high-frequency data collection

The Selke River, central Germany, has a drainage area of 456 km^2. It is part of the TERENO (TERrestrial ENvironmental Observatories) project (http://www.tereno.net/overview-de, last accessed October 31, 2018). The elevation ranges from 605 m in the upper mountains to 53 m in the lowlands. The two study reaches are located upstream of the gauging stations Meisdorf and Hausneindorf, representing the dominant forested and agricultural land, respectively (**Figure 1**). Due to gradients of meteorological and geomorphological conditions, the catchment is characterized by high hydrological heterogeneity (**Table S1**). Due to highly fertile soils, the agricultural land is dominated by arable land cropped mainly with winter wheat, winter barley and maize. Pasture accounts only for 3.5% of total catchment area and is exclusively located in the upper part of the catchment. Agricultural streams are mostly characterized by open canopy. This is confirmed by a detailed survey from the State Agency for Flood Protection and Water Management of Saxony-Anhalt (LHW) on riparian vegetation using 100 m stream segment. At the two largest agricultural tributaries of the Selke River (i.e., the Getel and the Hauptseegraben, **Figure S1**), only 6% of the surveyed stream segments have gallery trees (80% of them occur only on one side of the stream). Most of the agricultural streams have no high riparian vegetation. Only the main stem of the lowland Selke River (4th and 5th order) is partly shaded by bushes and riparian gallery trees. The open canopy allows high irradiance at the water surface and the subsequent development of large mats of periphyton and macrophytes (Rode et al. 2016a).

Figure 1. near here

Figure 1. The Selke catchment, river network and land cover types. Multi-parameter sensors were deployed at station Hausneindorf and station Meisdorf, representing agricultural and forest streams, respectively.

The outlet station Hausneindorf measures flow and NO_3^- dynamics of the entire catchment. Reaches upstream of this station represent open or very-sparse canopy agricultural streams. Upstream reaches of the station Meisdorf are mostly forest streams, of which riparian zones are dominated by trees with a closed-canopy during the vegetation period. In the lowland streams, NO_3^- concentrations are much higher than those in the upper streams (values of biweekly grab samples 1997-2015 at the two stations are 3.61 ± 1.09 and 1.60 ± 1.00 $mg\ l^{-1}$, respectively) due to long-term agricultural activities. Concentrations of soluble reactive phosphorus (SRP) are similarly high (0.040 ± 0.022 $mg\ l^{-1}$) at both stations.

Multi-parameter sensors (YSI 610 and TRIOS ProPS-UV) were deployed at the two stations. We continuously measured dissolved oxygen (DO), water temperature, pH, turbidity (only available in 2015) and NO_3^- concentration at a 15-min interval. The quality of high-frequency sensor NO_3^- measurements was validated using parallel grab samples (see Rode et al. (2016a)). We collected five years of data (from January 1, 2011 to December 31, 2015) from the two stations. High-frequency discharge and air pressure data were collected from the state agency (LHW) and the German Weather Service, respectively. For more details on the high-frequency monitoring and maintenance, refer to Rode et al. (2016a).

2.2. Calculation of metabolism rates and NO_3^- uptake rate

Daily GPP ($g\ O_2\ m^{-2}\ d^{-1}$) and ecosystem respiration (ER, $g\ O_2\ m^{-2}\ d^{-1}$) from 15-min DO measurements were calculated based on the single-station method (Odum 1956). The determination of the reaeration coefficient is one of the key issues in metabolic calculation (Raymond et al. 2012). The energy dissipation method (Bott et al. 2006, Tsivoglou and Neal 1976) was used in this study, which has been evaluated with a propan tracer test in the study site (Rode et al. 2016a). DO saturation percentage was determined from the measured DO concentration, water temperature and barometric pressure. Rates of GPP and ER were calculated using the measured DO differences between consecutive 15-min records, considering the effects of DO saturation deficit and reaeration. Day-time ER was assumed to be equal to the night-time ER. Daily net ecosystem production (NEP) was calculated as daily $GPP - ER$. For more details on the calculation, please refer to the Supplementary Materials. Values during over-bank flow periods (discharge > 7 $m^3 s^{-1}$) were not considered, and unrealistic negative GPP and ER values were omitted (11% and 14% for Meisdorf and Hausneindorf, respectively). For detailed quality control of metabolism rate calculation, refer to Rode et al. (2016a).

Theoretically, $U_{a-NO_3^-}$ ($mg\ N\ m^{-2}\ d^{-1}$) can be obtained directly from the diel amplitude of NO_3^- concentration (i.e., measured $U_{a-NO_3^-}$, modified from Heffernan and Cohen (2010)):

$$U_{a-NO_3^-} = \frac{1}{A}\sum_{t=0}^{n}[Q_t \cdot ([NO_3^{-1}]_{\max(0)} - [NO_3^{-1}]_t)] \tag{1}$$

where $[NO_3^-]_{\max(0)}$ and $[NO_3^-]_t$ ($mg\ l^{-1}$) denote the preceding predawn peak of NO_3^- concentration and NO_3^- concentration at time step t, respectively; Q_t ($l\ s^{-1}$) denotes discharge at time step t; A denotes benthic area (m^2), which is estimated from the reaeration coefficient and flow velocity measured upstream of each gauging station (Rode et al. 2016a); and n denotes the number of measurements per diel change.

As mentioned by Hensley and Cohen (2016) and Rode et al. (2016a), upstream effects propagate over a longer distance for NO_3^- than for DO and the diel change of NO_3^- can be disturbed rapidly by additional upstream inputs. Therefore, the measured $U_{a-NO_3^-}$ from diel amplitudes of NO_3^- concentration can only be obtained during steady low-flow conditions. Based on the five years of measurements, we defined the regression between measured $U_{a-NO_3^-}$ and GPP to obtain continuous daily $U_{a-NO_3^-}$ calculations (i.e., GPP-based $U_{a-NO_3^-}$ calculations).

2.3. Stream surface light availability and the $U_{a-NO_3^-}$ regionalization approach

Light availability near the stream surface is increased by PAR above the canopy and decreased by shading of riparian vegetation. We collected daily sunshine duration data from the Ummendorf weather station (35 km north of the Hausneindorf station) and calculated the theoretical daily GR (Allen et al. 1998) from 2011-2015. For details on the GR calculation, please refer to the Supplementary Materials. Since the daily series of

GR fluctuated greatly, we smoothed the data using a 5-day moving average method and obtained averaged daily global radiation $GR_{\bar{t}}$ ($MJ\ m^{-2} d^{-1}$). The time window of 5 days was arbitrarily chosen to balance the trends and fluctuations. The impact of GR on light availability was calculated by min-max normalization of the smoothed GR data (feature scaling):

$$f_{GR,t} = \frac{GR_{\bar{t}} - \min\left(GR_{\bar{t}\in[1,n]}\right)}{\max\left(GR_{\bar{t}\in[1,n]}\right) - \min\left(GR_{\bar{t}\in[1,n]}\right)} \tag{2}$$

where $f_{GR,t} \in [0,1]$ denotes the GR coefficient at time t; $\max\left(GR_{\bar{t}\in[1,n]}\right)$ and $\min\left(GR_{\bar{t}\in[1,n]}\right)$ denote the maximum and minimum $GR_{\bar{t}}$ values, respectively; and n denotes the day number of the time series. Field measurements of GR and PAR in a nearby weather station (Wulferstädt station, 2013-2015) showed a strong linear relationship between GR and PAR ($PAR = 0.64 \times GR$, $R^2 = 0.98$) and agreement between calculated GR at Ummendorf and measured GR at Wulferstädt ($R^2 = 0.96$, **Figure S2**). Normalization also eliminated the scale effect. Therefore, we used GR directly, instead of PAR.

We assumed that riparian vegetation is the same as that in the surrounding landscape. Therefore, the condition of the riparian vegetation was represented by land cover type. Leaf area index (LAI) was chosen to represent spatiotemporal distribution of the riparian canopy. The negative impact of riparian shading on light availability was calculated by min-max normalization of LAI among all land cover types (i.e., the riparian shading coefficient). To simplify preparation of LAI data, we calculated generic daily LAI values for each land cover type using the mean monthly values and applied each annual pattern for all five years. When year-to-year LAI changes significantly, the measured values or remote sensing data are recommended.

The overall stream surface light availability was calculated as:

$$f_{L,t}^{j} = f_{GR,t} \cdot (1 - \sum_{i=1}^{k} \alpha_j^i \cdot f_{LAI,t}^{i}) \tag{3}$$

where $f_{L,t}^{j} \in [0,1]$ denotes the overall coefficient of near surface light availability of stream segment j at time t; $f_{LAI,t}^{i} \in [0,1]$ denotes the riparian shading coefficient of land cover type i; and α_j^i denotes the areal proportion of each land cover type i surrounding stream segment j. From grid-based modeling perspective, one stream segment was defined for each modeling grid cell. Therefore, α_j^i was equivalent to the length proportion of each riparian vegetation type. We further assumed that no significant shading for streams surrounded by non-forest types (e.g., agricultural streams) and set $f_{LAI,t}^{i}$ values of these stream segments to zero.

The light availability coefficient ($f_{L,t}^{j}$) provides a spatiotemporal estimate of the combined impact of GR and riparian shading. Therefore, $U_{a-NO_3^-}$ was simply quantified as:

$$U_{a-NO_3^-,t}^{j} = U_{a,max} \cdot f_{L,t}^{j} \tag{4}$$

where $U_{a-NO_3^-,t}^{j}$ denotes $U_{a-NO_3^-}$ of stream j at time t, and $U_{a,max}$ denotes the general parameter (i.e., the potential uptake rate). This parameter can be explained physically as the $U_{a-NO_3^-}$ value under optimal GR conditions (e.g., on clear-sky dates with the longest sunshine duration of the year). Based on this parsimonious approach, $U_{a-NO_3^-}$ and its spatiotemporal variability can be easily obtained based on commonly available data (i.e., GR, LAI and land cover information).

2.4. The grid-based mHM-Nitrate model and networked upscaling

The mHM-Nitrate model is a fully distributed catchment nitrate model (Yang et al. 2018). The model is developed on the multi-scale platform of the mHM model (Samaniego et al. 2010). The mHM-Nitrate model provides reliable spatial simulations of hydrological and nitrate fluxes, as well as spatial details of physical and environmental characteristics of the catchment. These characteristics are upscaled from basic geographical data levels to the modeling level using the multi-scale parameter regionalization procedure (Samaniego et al. 2010). Each stream segment contains a complete set of flow routing and nitrate processing (i.e., assimilatory uptake, mineralization and denitrification). Therefore, stream morphological information can be linked directly to simulating NO_3^- transport and uptake processes.

The new approach of $U_{a-NO_3^-}$ regionalization (Eqs. 2 - 4) was integrated into the mHM-Nitrate model. Since assimilated nitrogen can be remineralized and return to the in-stream nitrate pool, mineralization was refined to equal a proportion of autotrophic NO_3^- uptake, while denitrification remained as that of the original mHM-Nitrate. The model was set up in the Selke catchment using a 1 km^2 cell size for both terrestrial and in-stream phases, and was calibrated against observations of the two gauging stations. Daily discharge and NO_3^- concentration were simulated and provided for each stream. The proportion of each land cover type in the area of each model cell was calculated using the basic land cover map (100 m resolution). Morphological characteristics were calculated for each stream, as follows: Stream length was calculated as the distance to the adjacent or diagonal cell based on the Digital Elevation Model (DEM, 100 m resolution) and summed up to the modeling level (1 km resolution); Stream width was estimated from simulated discharge, based on the empirical equation by Rode et al. (2016a). GR data from the Ummendorf station were used for the entire catchment. We matched the modeled river network to the real network that generated from the DEM and modified according to topographical maps (source from the State Agency for Survey and Geoinformation of Sachsen-Anhalt, Germany). We assigned model simulations to corresponding streams in the real network. The main stem of the Selke River from the modeled network was used for the daily longitudinal analysis (**Figure S1**).

2.5 Approach validation at reach scale and statistical analysis methods

The approach was firstly validated using the daily GPP-based $U_{a-NO_3^-}$ calculations from the agricultural stream (station Hausneindorf). Potential outliers in the calculations were detected using the interquartile range (IQR) method, and the $U_{a,max}$ value was assigned as 1.5 IQR of the upper quartile (ca. 99.65%). This parameter value was then applied directly to the forest stream (station Meisdorf), whose daily $U_{a-NO_3^-}$ calculations were used to validate the performance of the approach and the transferability of the parameter under different riparian conditions.

To evaluate the spatial pattern and seasonality of modeled autotrophic NO_3^- uptake, each stream was identified by three attributes: stream order, riparian vegetation type and mean uptake values of each season. We summarized three types of vegetation at the modeling level: agriculture (streams surrounded by > 80% of agricultural land), forest (streams surrounded by > 80% of forest) and mixture (all other streams). Analysis of variance (ANOVA) was conducted using *R software* (R Core Team 2017). Normality of the data was ensured using log-transformation, and homogeneity of variance was tested using the Levene's test (results not shown). Significant ANOVA results ($p < 0.01$) were examined further using post-hoc test (Tukey's Test) for pairwise comparisons. The *beta* coefficient (*lm.beta* package in *R*) was calculated to identify the most descriptive attributes (higher absolute *beta* value indicates a stronger effect).

3. Results and Discussion

3.1. Metabolism rates and GPP-based $U_{a-NO_3^-}$ calculations

In the agricultural stream (**Figure 2**), GPP (mean ± standard deviation (SD) = 2.10 ± 1.78 $g\ O_2\ m^{-2} d^{-1}$) was moderately correlated with GR ($R^2 = 0.42, p < 0.01$) and therefore generally peaked in summer. ER (mean ± SD = 3.28 ± 1.75 $g\ O_2\ m^{-2} d^{-1}$) was slightly higher than GPP but within the same order of magnitude. It was also correlated with global radiation ($R^2 = 0.33, p < 0.01$), but the correlation was sometimes influenced by flooding events. NEP was generally close to zero (mean = - 1.10 ± 1.83 $g\ O_2\ m^{-2} d^{-1}$), with slightly positive values in spring (0.50 ± 2.03 $g\ O_2\ m^{-2} d^{-1}$) and mostly negative values in late autumn (-2.38 ± 1.10 $g\ O_2\ m^{-2} d^{-1}$). Results generally agreed with the first two-year calculation by Rode et al. (2016a). However, seasonal patterns of metabolism rates in the last three years were more diverse. For instance, during the months of June-October, GPP was significantly lower in 2014-2015 than in 2011-2013 (mean = 1.66 vs. 2.74 $g\ O_2\ m^{-2} d^{-1}$, respectively; ANOVA, $p < 0.01$). In 2014, comparable degree of reductions in GPP and ER were observed and mean NEP

(- 0.97 $g\ O_2\ m^{-2}d^{-1}$) was similar to the annual mean value. The reductions may be attributed to higher discharge during the dry months (mean = 1.26 vs. 0.62 m^3s^{-1} for other years) which increases bottom shear stress, possibly resulting in moderate removal of benthic communities. Biofilm aging and algal sloughing may also contribute to the reduction in both GPP and ER during moderate flow (Uehlinger 2006). In 2015, GPP decreased more than ER, resulting in higher negative NEP (mean = - 2.04 vs. - 1.22 $g\ O_2\ m^{-2}d^{-1}$ for other years). Turbidity is the most likely cause of this stronger decrease in GPP than in ER (**Figure S3**). Increased turbidity reduces the amount of light that penetrates from the surface to the riverbed, while the fine sediments being transported stimulate respiration due to their high concentrations of labile organic carbon (O'Connor et al. 2012, Roberts et al. 2007).

Figure 2. near here

Figure 2. Daily metabolism rates (i.e., gross primary production-GPP, ecosystem respiration-ER and net ecosystem production-NEP) at Hausneindorf, representing typical agricultural streams. ER was shown as negative values for better visibility.

Metabolism rates in the forest stream (**Figure S4**) had distinctly different behavior than those in the agricultural stream. GPP (mean ± SD = 0.54 ± 0.62 $g\ O_2\ m^{-2}d^{-1}$) was significantly lower (ANOVA, $p < 0.01$), and the seasonal pattern differed completely. It increased in spring due to the increase in GR and peaked (mean = 2.85 $g\ O_2\ m^{-2}d^{-1}$) at the beginning of May, when significant shading from riparian vegetation occurred. In the following month, GPP decreased dramatically to a low level (mean = 0.25 $g\ O_2\ m^{-2}d^{-1}$) and remained low until late autumn. After litterfall, GPP increased slightly (e.g., in 2013-

2015), but the increase was low due to the already reduced GR in late autumn (Roberts et al. 2007). ER (mean ± SD = 4.65 ± 5.61 $g\ O_2\ m^{-2}d^{-1}$) was generally much higher than GPP, indicating strong net heterotrophic behavior in the forest stream ($NEP < 0$ throughout the year). The seasonal ER pattern was more diverse, with generally higher values in winter and spring and high variability throughout the year. ER was correlated with stream flow ($R^2 = 0.60, p < 0.01$), most likely because ER can be stimulated by hydrological events which provide more allochthonous labile organic inputs (Mulholland et al. 2001).

Linear regressions between measured $U_{a-NO_3^-}$ and GPP at stations Hausneindorf and Meisdorf (n = 90 and 67, respectively, **Figure 3**) were similar to those of a former study using the first two years of data (2011-2012) (Rode et al. 2016a). This demonstrated that the correlation was robust in the Selke catchment.

Figure 3. near here

Figure 3. Linear regressions between measured autotrophic NO_3^- uptake ($U_{a-NO_3^-}$) and GPP at (a) Hausneindorf and (b) Meisdorf, representing the agricultural and forest streams, respectively, during low flow conditions (discharge$< 0.8\,m^3\ s^{-1}$).

3.2. Performance of the $U_{a-NO_3^-}$ regionalization approach

The GR coefficient (**Figure S5a**) showed a clear seasonal pattern with considerable differences among years (e.g., unimodal or multimodal). The shading coefficient based on LAI (**Figure S5b**) demonstrated clear differences in shading among forest types: deciduous trees provided the highest shading in July-August and almost no shading before leaf-out and after litterfall; conifers provided constant high shading throughout the year; and the other forest types in the Selke catchment provided intermediate levels of shading. Based on our assumptions, non-forest shading was set to zero. The overall light coefficient (Eq. 3) for each stream depended on the proportions of each land cover type (see an example in **Figure S5c**).

Daily GPP-based $U_{a-NO_3^-}$ calculations for agricultural and forest streams (Hausneindorf and Meisdorf, respectively, **Figure 4**) were estimated based on continuous daily GPP and correlations between measured $U_{a-NO_3^-}$ and GPP, respectively. The potential uptake rate ($U_{a,max}$) was determined as 283 $mg\ N\ m^{-2} d^{-1}$ based on the dataset from Hausneindorf (n = 1563, **Figure S6**). For the open-canopy agricultural stream, simulations from the regionalization approach reproduced the seasonal pattern of the calculated $U_{a-NO_3^-}$ relatively well (**Figure 4a**), especially in the first two years, when discharge in low-flow periods was relatively low and stable. In 2013, GPP-based $U_{a-NO_3^-}$ calculations were extremely high (≥ 300 $mg\ N\ m^{-2} d^{-1}$) during March-June (i.e., the off-set and in-between periods of two extreme flooding events). Simulations underestimated by more than 50%. The higher discharge (mean = 2.50 $m^3\ s^{-1}$) and lower temperature (ca. 4 ℃ lower than the daily mean) during these periods might have introduced high uncertainty in metabolism rate calculations (Riley and Dodds 2012). Similarly, in March 2014 and 2015, measured $U_{a-NO_3^-}$ (mean = 66.6 $mg\ N\ m^{-2} d^{-1}$, n=12) were similar to the simulations (mean = 76.1 $mg\ N\ m^{-2} d^{-1}$, n=62), but much lower than the GPP-based calculations (mean = 131.5 $mg\ N\ m^{-2} d^{-1}$, n=59). This further suggests that uncertainty in calculated metabolism rate may increase with increased discharge.

We determined the proportion (α) of each land cover type in a 1 km^2 area surrounding Meisdorf, i.e., coniferous forest (0.00), deciduous forest (0.52), mixed forest (0.25) and pasture (0.23). The simulated $U_{a-NO_3^-}$ reproduced the range and seasonal pattern of GPP-based calculations remarkably well (**Figure 4b**). Although we observed discrepancies for the agricultural stream and transferred the potential uptake rate directly to the forest stream, the approach clearly captured the large differences of calculated $U_{a-NO_3^-}$ between the two riparian conditions. Slight overestimates occurred from May-June, most likely due to aspect shading from the steep valley alongside the stream (Bernhardt et al. 2018). The approach missed several observed spikes, which likely correspond to pulses of discharge and turbidity. The dramatic decrease in calculated $U_{a-NO_3^-}$ in 2012 is probably due to the sharp decrease in water temperature (Rode et al. 2016a).

Figure 4. near here

Figure 4. GPP-based calculations and approach simulations of the N uptake rate (i.e., $U_{a-NO_3^-}$) at (a) Hausneindorf and (b) Meisdorf, representing the agricultural and forest streams, respectively.

In addition to the visual consistency in seasonal patterns, the simulations correlated reasonably with the GPP-based $U_{a-NO_3^-}$ calculations ($R^2 = 0.47 \text{ and } 0.45$ for Hausneindorf and Meisdorf, respectively), given the parsimony of the approach and the distinct uptake behaviors at the two sites. Therefore, light can be identified as the main factor influencing the seasonal autotrophic NO_3^- uptake in the Selke River. Other influential factors were similar at the two sites. The C/N ratios of benthic biofilm were similar (8.7 and 8.5 for the agricultural and forest streams, respectively) (Kamjunke et al. 2015). From June-October, water temperature was 14.2 ± 4.3 and 12.0 ± 4.2 ℃, respectively, which is sufficient in supporting high growth rates of diatoms (Anderson 2000).

We assumed that riparian vegetation is the same as the surrounding landscape. This assumption is validated by the LHW survey data in the catchment. Although the lowland main stem of the Selke is dominated by sparse gallery trees, GPP values at Hausneindorf are comparable with values reported in other agricultural streams (e.g., Beaulieu et al. (2013) and Griffiths et al. (2013)) and the approach performed well. This indicates that the gallery trees do not provide sufficient shading on the stream surface, presumably due to the relatively large side-to-side distance and less shading density of the trees. Still, the assumptions might not completely valid for agricultural or urban streams with a significant buffer of trees planted along the stream corridor. However, such information is rarely available at river network scale (e.g., resolution mismatching of satellite data and expensive to survey all tributaries) and extrapolating the shading effect from on-site measurements remains challenging (Davies-Colley and Rutherford 2005).

Our regionalization approach focuses on quantifying stream surface light availability. Other factors are not included in its design. Water temperature is not explicitly considered because it is not available network wide, and spatiotemporal estimates of water temperature can be quite uncertain. The impact of water temperature is partly considered by light and is more relevant for ER than for GPP (Demars et al. 2011). Turbidity decreases the amount of light that penetrates to benthic areas (Julian et al.

2008), which likely resulted in the overestimation of the simulated $U_{a-NO_3^-}$ in the summer/autumn periods of 2014-2015. Based on the continuous measurements in 2015 (**Figure S3**), we observed a plausible correspondence between the increase in turbidity and the decrease in GPP, but the relationship is quantitatively unclear, let alone linking turbidity to widely available discharge data for regionalization purposes. Flow disturbance likely has significant episodic impact on stream metabolism, following a threshold behavior (O'Connor et al. 2012, Uehlinger 2006). The resilience of GPP to flow disturbance is suspected to be relatively quick, especially in high PAR seasons, except for highly complicated cases in which successive disturbances occur (O'Connor et al. 2012). The impact of flow disturbance is mechanistically controlled by turbulence and sediment interactions (O'Connor et al. 2012), which are challenging to determine and require adequate descriptions of hydraulics and sediment properties. Therefore, flow disturbance is excluded from the approach. Nutrient limitation may constraint the autotrophic uptake in certain cases. However, the relationship between nutrient supply and GPP increase is also reported as weak (Bernot et al. 2010), most likely due to the already high nutrient levels in anthropogenically impacted streams.

3.3. Network upscaling and spatiotemporal variability of NO_3^- uptake

Integrating the approach into mHM-Nitrate model predicted a strong spatial variability of seasonal mean $U_{a-NO_3^-}$ (**Figure S7**). Agricultural streams had much higher uptake rates than forest streams (mean ± SD = 86.4 ± 1.9 vs. 18.8 ± 6.2 $mgNm^{-2}d^{-1}$, respectively) due to less riparian shading. The differences between the two main riparian vegetation types were much smaller in winter (10.1 ± 0.42 vs. 4.6 ± 2.2 $mg\ N\ m^{-2}d^{-1}$) probably due to the universally low winter GR. The higher SD for forest streams indicated more diverse uptake patterns due to different shading patterns (represented by different LAI patterns) in different forest types. We used only basic information (i.e., global radiation, LAI and land cover information), but did provide the varied seasonality of $U_{a-NO_3^-}$ under different light regimes.

By multiplying modeled stream benthic areas, seasonal mean gross NO_3^- uptake ($U_{ass}, kg\ N\ d^{-1}$) was calculated for each stream in the network (**Figure 5**). The coefficient of variance (CV) of U_{ass} was much higher than that of $U_{a-NO_3^-}$ (CVs of annual mean = 1.51 and 0.57, respectively), indicating a higher overall spatial variability. Due to variations in stream morphological properties, U_{ass} varied among areas with the same shading condition. Two-way ANOVA showed that U_{ass} varied significantly among different stream orders and vegetation types in all seasons. A post-hoc test (Tukey's test) identified that the U_{ass} of 1st (annual mean = 0.27 $kg\ N\ d^{-1}$) and 2nd (0.51 $kg\ N\ d^{-1}$) order streams was significantly lower than that of higher orders (1.77 $kg\ N\ d^{-1}$ for all 3rd -5th order streams) due to flow accumulation in higher order streams. The U_{ass} of forest streams differed significantly from those of agricultural and mixed streams, except in winter, when all values were low. U_{ass} also showed significant seasonal variability in all streams (ANOVA, $p < 0.01$). However, Post-hoc test revealed that mean values in spring and summer differed significantly only in forest streams. The differences in agricultural and mixed streams (p = 0.50 and 0.93, respectively) attenuated due to the larger benthic area in spring, albeit generally higher $U_{a-NO_3^-}$ in summer. The *beta* coefficients indicated that season and stream order had the greatest effect on U_{ass}, whereas season and vegetation type had the greatest effect on $U_{a-NO_3^-}$.

Figure 5. near here

Figure 5. Seasonal mean gross NO_3^- uptake amount (U_{ass}) at the Selke river network. The color ramp of the legend within the range of [0,1] $kg\ N\ d^{-1}$ was zoomed in on the right side.

We used the detailed spatial simulations of nitrate loads ($L_{NO_3^-}, kg\ N\ d^{-1}$) from the mHM-Nitrate model (**Figure S8**) to calculate the uptake efficiency (i.e., the uptake percentage, $U_P = U_{ass}/L_{NO_3^-} \times 100$) for each stream in the network. U_P peaked in summer (mean ± SD = 21.4 ± 17.8%), when the highest U_{ass} encountered the lowest $L_{NO_3^-}$ (**Table S2**), whereas in winter, U_P values were extremely low throughout the river network (1.0 ± 1.7%) due to the high $L_{NO_3^-}$ and low U_{ass}. U_P was consistently lower in higher order streams (e.g., annual means were ca. 14% and 4% in 1st and 4th order streams, respectively), mainly due to the greater increase in $L_{NO_3^-}$ than in U_{ass} with increasing stream order. However, all pairs of adjacent stream orders (i.e., 1st-2nd, 2nd-3rd and 3rd-4th) did not differ significantly ($p > 0.01$) in summer. This can be attributed to the consistently low $L_{NO_3^-}$ from 1st to 4th order streams in summer (mean = 5 to 55 $kg\ N\ d^{-1}$, respectively).

Longitudinal daily U_P in the main stem of the Selke clearly showed the strong impact of riparian vegetation on U_P seasonal dynamics and its inter-annual variation (**Figure 6**). Critical locations and periods of high NO_3^- uptake percentage (e.g., $>$ 40%) could be explicitly identified. The critical period was longer in upper agricultural streams (≥ 23 km from the outlet) than in lower agricultural streams (≤ 11 km from the outlet). The shallow impermeable bedrock in the upper Selke catchment results in a preference of flashier flow path, which prevents NO_3^- accumulation in the soil (Dupas et al. 2017). Whereas loess sediments dominate the lower agricultural part of the catchment and NO_3^- concentration in the soil can reach up to ca. 40 $mg\ l^{-1}$ due to agricultural activities (Yang et al. 2018). Therefore, $L_{NO_3^-}$ was much lower in the upstream of the Selke River than in the downstream, especially during baseflow dominant periods. This presumably prolonged the periods of high uptake percentage in the upper agricultural streams. U_P in forest streams (ca. 12-22 km from the outlet) generally increased from winter to spring and peaked in May or June, then sharply decreased to a low level (mean = 3%). Seasonal dynamics of U_P differed among years, depending on the spatiotemporal combination of $L_{NO_3^-}$ and U_{ass}. The spatial distributions and temporal dynamics of $L_{NO_3^-}$ had more influence on U_P due to its higher order of magnitude, compare to those of U_{ass}. In lowland agricultural streams, the period of high uptake percentage in 2011 was much more pronounced in streams upstream of the confluence than downstream, where the Getel stream joins the main Selke (**Figure 6**). This is due to much lower $L_{NO_3^-}$ from the upper Selke stream in June-October of 2011 (mean load = 41.6 vs. 107.3 $kg\ N\ d^{-1}$ for the five-year mean of this dry period) and higher relative contribution of $L_{NO_3^-}$ from the Getel stream (32% vs. 15% for the five-year mean).

Figure 6. near here

Figure 6. Longitudinal daily dynamics of the uptake percentage (U_P) in the main stem of the Selke (marked in Figure S2). The width of each horizontal band indicates the length of each stream. The gray dashed line identifies the location where stream Getel joins the main Selke.

3.4. Implications

An increasing number of water quality parameters, such as pH, DO, turbidity, NO_3^- and SRP, can be measured at high temporal resolution by sensors. The new data thus provide potential insights of in-stream processes at reach scale (Rode et al. 2016b). However, regionalizing those processes remains challenging, because in-stream processes (e.g., NO_3^- assimilation and remineralization) always interact intensively, and only a few can be individually linked to observations (e.g., the autotrophic NO_3^- uptake in this study). Therefore, novel reach-scale experimental designs are needed in current/future research to provide direct measurements of individual processes. e.g., A new reach scale mass balance approach by Kunz et al. (2017) can potentially be used to regionalize the in-stream denitrification process.

In the regionalization procedure, the selection of key environmental factors is critical at both reach and network scales. There is a high risk of over-parameterizing approaches based on reach-scale understandings. We are unable to consider certain influential factors due to data limitations, and catchment-scale behavior might be simpler than that expected from detailed process understanding (Jackson-Blake et al. 2017). Therefore, a parsimonious approach can be an appropriate initial step for upscaling issues (Kirchner 2006). Specifically, the parsimony of an approach is reflected, in our opinion, in two perspectives: (1) input data requirements (i.e., the applicability of an approach depends largely on the input data it requires and the accessibility of these data) and (2) the parameterization (i.e., the introduced parameter should be easily identifiable and transferable with clear physical meaning). The proposed regionalization of $U_{a-NO_3^-}$ used only GR, LAI and land cover data, which are widely available for entire catchment, but quantified spatiotemporal variations in stream surface light regimes well. The physical meaning of the parameter $U_{a,max}$ indicates that it can be measured directly by traditional field experiments and be transferred to regions with similar radiation condition.

4. Conclusions

- Five-year continuous high-frequency measurements revealed strong correlations between in-stream autotrophic NO_3^- uptake and ecosystem metabolism (specifically GPP), and distinct seasonal behaviors in forest and agricultural streams were observed in this study.
- A parsimonious approach was proposed to quantify stream surface light availability (i.e., using basic GR, LAI and land cover information) and to regionalize $U_{a-NO_3^-}$. The approach performed well in terms of capturing seasonal variations and improving spatial transferability to different riparian shading conditions.
- The parsimonies of data requirements and parameterization suggest that the approach has a strong upscaling capability. By integrating the approach into the fully distributed mHM-Nitrate model, more detailed spatiotemporal variability of NO_3^- transport and uptake could be investigated at river network scale, which is informative in guiding water quality management.
- This study provides a working procedure for regionalizing in-stream process understandings inspired from new high-frequency data and upscaling such reach-scale findings to river network scale using fully distributed catchment models.

Acknowledgements

Xiaoqiang Yang is funded by the Chinese Scholarship Council (CSC). We would like to thank Dr. Daniel Graeber and Dr. Robert Hensley for their constructive comments and discussions. We highly appreciate the comments from the Editor and the anonymous Reviewers, which helped us to improve the manuscript significantly. This research is supported by the TERENO (TERrestrial ENvironmental Observatories) project. We thank the German Weather Service (DWD) for providing meteorological data, State Agency for Flood Protection and Water Management of Saxony-Anhalt (LHW) for providing discharge and riparian vegetation survey data, State Agency for Survey and Geoinforamtion of Saxony-Anhalt for providing topographic maps, and Dr. Corinna Rebmann (Helmholtz Centre for Environmental Research - UFZ) for sharing the radiation measurements (photosynthetically active radiation and global radiation) at station Wulferstädt.

References

Alexander, R.B., Böhlke, J.K., Boyer, E.W., David, M.B., Harvey, J.W., Mulholland, P.J., Seitzinger, S.P., Tobias, C.R., Tonitto, C. and Wollheim, W.M. (2009) Dynamic modeling of nitrogen losses in river networks unravels the coupled effects of hydrological and biogeochemical processes. Biogeochemistry 93(1), 91-116, https://doi.org/10.1007/s10533-008-9274-8.

Allen, R.G., Pereira, L.S., Raes, D. and Smith, M. (1998) Crop evapotranspiration - Guidelines for computing crop water requirements, FAO - Food and Agriculture Organization of the United Nations, Rome, Italy.

Anderson, N.J. (2000) Miniview: Diatoms, temperature and climatic change. European Journal of Phycology 35(4), 307-314, https://doi.org/10.1080/09670260010001735911.

Beaulieu, J.J., Arango, C.P., Balz, D.A. and Shuster, W.D. (2013) Continuous monitoring reveals multiple controls on ecosystem metabolism in a suburban stream. Freshwater Biology 58(5), 918-937, https://doi.org/10.1111/fwb.12097.

Bernhardt, E.S., Heffernan, J.B., Grimm, N.B., Stanley, E.H., Harvey, J.W., Arroita, M., Appling, A.P., Cohen, M.J., McDowell, W.H., Hall, R.O., Read, J.S., Roberts, B.J., Stets, E.G. and Yackulic, C.B. (2018) The metabolic regimes of flowing waters. Limnology and Oceanography 63(S1), S99-S118, https://doi.org/10.1002/lno.10726.

Bernhardt, E.S., Likens, G.E., Hall, R.O., Buso, D.C., Fisher, S.G., Burton, T.M., Meyer, J.L., McDowell, W.H., Mayer, M.S., Bowden, W.B., Findlay, S.E.G., Macneale, K.H., Stelzer, R.S. and Lowe, W.H. (2005) Can't See the Forest for the Stream? In-stream Processing and Terrestrial Nitrogen Exports. BioScience 55(3), 219-230, https://doi.org/10.1641/0006-3568(2005)055[0219:ACSTFF]2.0.CO;2.

Bernot, M.J., Sobota, D.J., Hall, R.O., Mulholland, P.J., Dodds, W.K., Webster, J.R., Tank, J.L., Ashkenas, L.R., Cooper, L.W., Dahm, C.N., Gregory, S.V., Grimm, N.B., Hamilton, S.K., Johnson, S.L., Mcdowell, W.H., Meyer, J.L., Peterson, B., Poole, G.C., Valett, H.M., Arango, C., Beaulieu, J.J., Burgin, A.J., Crenshaw, C., Helton, A.M., Johnson, L., Merriam, J., Niederlehner, B.R., O'Brien, J.M., Potter, J.D., Sheibley, R.W., Thomas, S.M. and Wilson, K. (2010) Inter-regional comparison of land-use effects on stream metabolism. Freshwater Biology 55(9), 1874-1890, https://doi.org/10.1111/j.1365-2427.2010.02422.x.

Bott, T.L., Montgomery, D.S., Newbold, J.D., Arscott, D.B., Dow, C.L., Aufdenkampe, A.K., Jackson, J.K. and Kaplan, L.A. (2006) Ecosystem metabolism in streams of the Catskill Mountains (Delaware and Hudson River watersheds) and Lower Hudson Valley. Journal of the North American Benthological Society 25(4), 1018-1044, https://doi.org/10.1899/0887-3593(2006)025[1018:Emisot]2.0.Co;2.

Davies-Colley, R.J. and Rutherford, J.C. (2005) Some approaches for measuring and modelling riparian shade. Ecological Engineering 24(5), 525-530, https://doi.org/10.1016/j.ecoleng.2004.01.006.

Demars, B.O.L., Russell, M.J., Ólafsson, J.S., Gíslason, G.M., Gudmundsdóttir, R., Woodward, G., Reiss, J., Pichler, D.E., Rasmussen, J.J. and Friberg, N. (2011) Temperature and the metabolic balance of streams. Freshwater Biology 56(6), 1106-1121, https://doi.org/10.1111/j.1365-2427.2010.02554.x.

Dupas, R., Musolff, A., Jawitz, J.W., Rao, P.S.C., Jäger, C.G., Fleckenstein, J.H., Rode, M. and Borchardt, D. (2017) Carbon and nutrient export regimes from headwater catchments to downstream reaches. Biogeosciences 14(18), 4391-4407, https://doi.org/10.5194/bg-14-4391-2017.

Ensign, S.H. and Doyle, M.W. (2006) Nutrient spiraling in streams and river networks. Journal of Geophysical Research: Biogeosciences 111(G4), https://doi.org/10.1029/2005JG000114.

Gomez-Velez, J.D., Harvey, J.W., Cardenas, M.B. and Kiel, B. (2015) Denitrification in the Mississippi River network controlled by flow through river bedforms. Nature Geoscience 8, 941-945, https://doi.org/10.1038/ngeo2567.

Grant, S.B., Azizian, M., Cook, P., Boano, F. and Rippy, M.A. (2018) Factoring stream turbulence into global assessments of nitrogen pollution. Science 359(6381), 1266-1269, https://doi.org/10.1126/science.aap8074.

Griffiths, N.A., Tank, J.L., Royer, T.V., Roley, S.S., Rosi-Marshall, E.J., Whiles, M.R., Beaulieu, J.J. and Johnson, L.T. (2013) Agricultural land use alters the seasonality and magnitude of stream metabolism. Limnology and Oceanography 58(4), 1513-1529, https://doi.org/10.4319/lo.2013.58.4.1513.

Heffernan, J.B. and Cohen, M.J. (2010) Direct and indirect coupling of primary production and diel nitrate dynamics in a subtropical spring-fed river. Limnology and Oceanography 55(2), 677-688, https://doi.org/10.4319/lo.2010.55.2.0677.

Helton, A.M., Poole, G.C., Meyer, J.L., Wollheim, W.M., Peterson, B.J., Mulholland, P.J., Bernhardt, E.S., Stanford, J.A., Arango, C., Ashkenas, L.R., Cooper, L.W., Dodds, W.K., Gregory, S.V., Hall, R.O., Hamilton, S.K., Johnson, S.L., McDowell, W.H., Potter, J.D., Tank, J.L., Thomas, S.M., Valett, H.M., Webster, J.R. and Zeglin, L. (2011) Thinking outside the channel: modeling nitrogen cycling in networked river ecosystems. Frontiers in Ecology and the Environment 9(4), 229-238, https://doi.org/10.1890/080211.

Hensley, R.T. and Cohen, M.J. (2016) On the emergence of diel solute signals in flowing waters. Water Resources Research 52(2), 759-772, https://doi.org/10.1002/2015WR017895.

Jackson-Blake, L.A., Sample, J.E., Wade, A.J., Helliwell, R.C. and Skeffington, R.A. (2017) Are our dynamic water quality models too complex? A comparison of a new parsimonious phosphorus model, SimplyP, and INCA-P. Water Resources Research 53(7), 5382-5399, https://doi.org/10.1002/2016WR020132.

Julian, J.P., Doyle, M.W. and Stanley, E.H. (2008) Empirical modeling of light availability in rivers. Journal of Geophysical Research: Biogeosciences 113(G3), https://doi.org/10.1029/2007JG000601.

Kamjunke, N., Mages, M., Büttner, O., Marcus, H. and Weitere, M. (2015) Relationship between the elemental composition of stream biofilms and water chemistry—a catchment approach. Environmental Monitoring and Assessment 187(7), 432, https://doi.org/10.1007/s10661-015-4664-6.

Kirchner, J.W. (2006) Getting the right answers for the right reasons: Linking measurements, analyses, and models to advance the science of hydrology. Water Resources Research 42(3), https://doi.org/10.1029/2005WR004362.

Kunz, J.V., Hensley, R., Brase, L., Borchardt, D. and Rode, M. (2017) High frequency measurements of reach scale nitrogen uptake in a fourth order river with contrasting hydromorphology and variable water chemistry (Weiße Elster, Germany). Water Resources Research 53(1), 328-343, https://doi.org/10.1002/2016WR019355.

Mulholland, P.J., Fellows, C.S., Tank, J.L., Grimm, N.B., Webster, J.R., Hamilton, S.K., Martí, E., Ashkenas, L., Bowden, W.B., Dodds, W.K., Mcdowell, W.H., Paul, M.J. and Peterson, B.J. (2001) Inter‐biome comparison of factors controlling stream metabolism. Freshwater Biology 46(11), 1503-1517, https://doi.org/10.1046/j.1365-2427.2001.00773.x.

Mulholland, P.J., Helton, A.M., Poole, G.C., Hall, R.O., Hamilton, S.K., Peterson, B.J., Tank, J.L., Ashkenas, L.R., Cooper, L.W., Dahm, C.N., Dodds, W.K., Findlay, S.E.G., Gregory, S.V., Grimm, N.B., Johnson, S.L., McDowell, W.H., Meyer, J.L., Valett, H.M., Webster, J.R., Arango, C.P., Beaulieu, J.J., Bernot, M.J., Burgin, A.J., Crenshaw, C.L., Johnson, L.T., Niederlehner, B.R., O'Brien, J.M., Potter, J.D., Sheibley, R.W., Sobota, D.J. and Thomas, S.M. (2008) Stream denitrification across biomes and its response to anthropogenic nitrate loading. Nature 452, 202-205, https://doi.org/10.1038/nature06686.

O'Connor, B.L., Harvey, J.W. and McPhillips, L.E. (2012) Thresholds of flow‐induced bed disturbances and their effects on stream metabolism in an agricultural river. Water Resources Research 48(8), https://doi.org/10.1029/2011WR011488.

Odum, H.T. (1956) Primary Production in Flowing Waters. Limnology and Oceanography 1(2), 102-117, https://doi.org/10.4319/lo.1956.1.2.0102.

R Core Team (2017) R: A Language and Environment for Statistical Computing, R Foundation for Statistical Computing, Vienna, Austria.

Raymond, P.A., Zappa, C.J., Butman, D., Bott, T.L., Potter, J., Mulholland, P., Laursen, A.E., McDowell, W.H. and Newbold, D. (2012) Scaling the gas transfer velocity and hydraulic geometry in streams and small rivers. Limnology and Oceanography: Fluids and Environments 2(1), 41-53, https://doi.org/10.1215/21573689-1597669.

Riley, A.J. and Dodds, W.K. (2012) Whole-stream metabolism: strategies for measuring and modeling diel trends of dissolved oxygen. Freshwater Science 32(1), 56-69, https://doi.org/10.1899/12-058.1.

Roberts, B.J. and Mulholland, P.J. (2007) In-stream biotic control on nutrient biogeochemistry in a forested stream, West Fork of Walker Branch. Journal of Geophysical Research: Biogeosciences 112(G4), https://doi.org/10.1029/2007JG000422.

Roberts, B.J., Mulholland, P.J. and Hill, W.R. (2007) Multiple Scales of Temporal Variability in Ecosystem Metabolism Rates: Results from 2 Years of Continuous Monitoring in a Forested Headwater Stream. Ecosystems 10(4), 588-606, https://doi.org/10.1007/s10021-007-9059-2.

Rode, M., Arhonditsis, G., Balin, D., Kebede, T., Krysanova, V., van Griensven, A. and van der Zee, S.E.A.T.M. (2010) New challenges in integrated water quality modelling. Hydrological Processes 24(24), 3447-3461, https://doi.org/10.1002/hyp.7766.

Rode, M., Halbedel née Angelstein, S., Anis, M.R., Borchardt, D. and Weitere, M. (2016a) Continuous In-Stream Assimilatory Nitrate Uptake from High-Frequency Sensor Measurements. Environmental Science & Technology 50(11), 5685-5694, https://doi.org/10.1021/acs.est.6b00943.

Rode, M., Wade, A.J., Cohen, M.J., Hensley, R.T., Bowes, M.J., Kirchner, J.W., Arhonditsis, G.B., Jordan, P., Kronvang, B., Halliday, S.J., Skeffington, R.A., Rozemeijer, J.C., Aubert, A.H., Rinke, K. and Jomaa, S. (2016b) Sensors in the Stream: The High-Frequency Wave of the Present. Environmental Science & Technology 50(19), 10297-10307, https://doi.org/10.1021/acs.est.6b02155.

Samaniego, L., Kumar, R. and Attinger, S. (2010) Multiscale parameter regionalization of a grid-based hydrologic model at the mesoscale. Water Resources Research 46(5), https://doi.org/10.1029/2008WR007327.

Tsivoglou, E.C. and Neal, L.A. (1976) Tracer Measurement of Reaeration: III. Predicting the Reaeration Capacity of Inland Streams. Journal (Water Pollution Control Federation) 48(12), 2669-2689, http://www.jstor.org/stable/25040082

Uehlinger, U. (2006) Annual cycle and inter‐annual variability of gross primary production and ecosystem respiration in a floodprone river during a 15‐year period. Freshwater Biology 51(5), 938-950, https://doi.org/10.1111/j.1365-2427.2006.01551.x.

Wollheim, W.M., Peterson, B.J., Thomas, S.M., Hopkinson, C.H. and Vörösmarty, C.J. (2008) Dynamics of N removal over annual time periods in a suburban river network. Journal of Geophysical Research: Biogeosciences 113(G3), https://doi.org/10.1029/2007JG000660.

Yang, X., Jomaa, S., Zink, M., Fleckenstein, J.H., Borchardt, D. and Rode, M. (2018) A new fully distributed model of nitrate transport and removal at catchment scale. Water Resources Research 54(8), 5856-5877, https://doi.org/10.1029/2017WR022380.

Ye, S., Reisinger, A.J., Tank, J.L., Baker, M.A., Hall Jr., R.O., Rosi, E.J. and Sivapalan, M. (2017) Scaling Dissolved Nutrient Removal in River Networks: A Comparative Modeling Investigation. Water Resources Research 53(11), 9623-9641, https://doi.org/10.1002/2017WR020858.

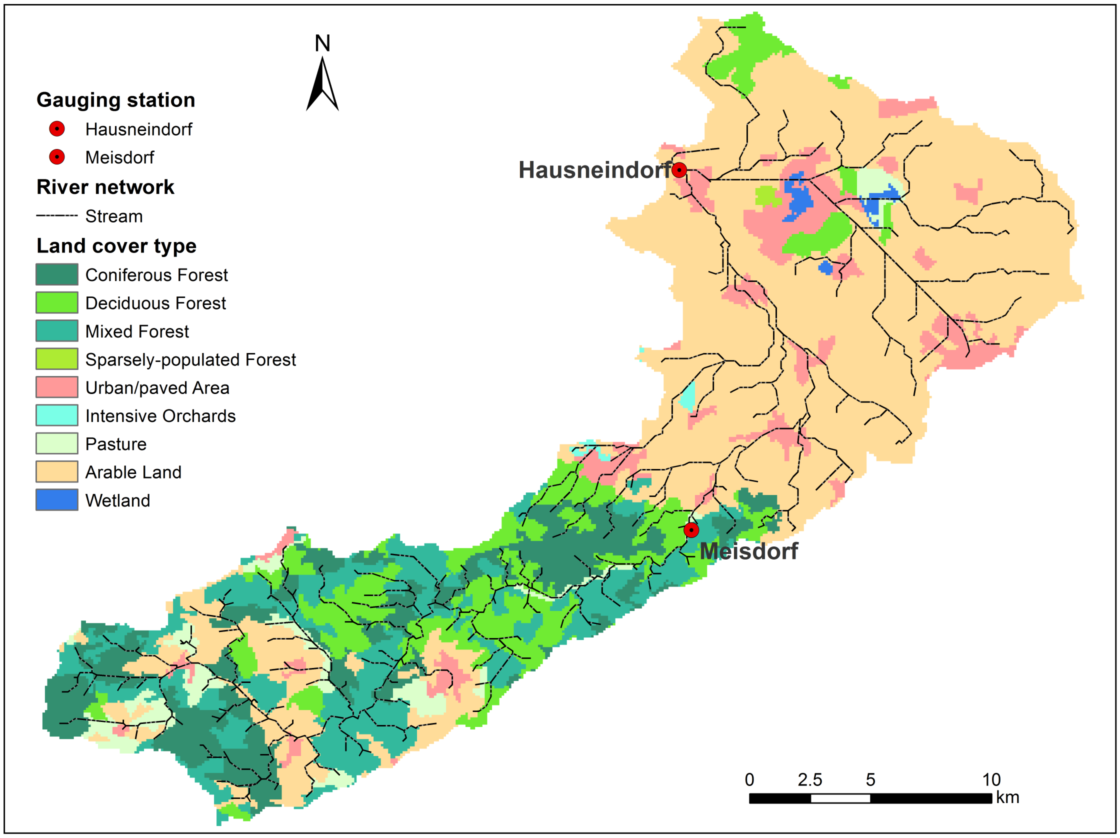
N
Gauging station
● Hausneindorf
● Meisdorf
River network
Stream
Land cover type
Coniferous Forest
Deciduous Forest
Mixed Forest
Sparsely-populated Forest
Urban/paved Area
Intensive Orchards
Pasture
Arable Land
Wetland
Hausneindorf
Meisdorf
0
2.5
5
10
km

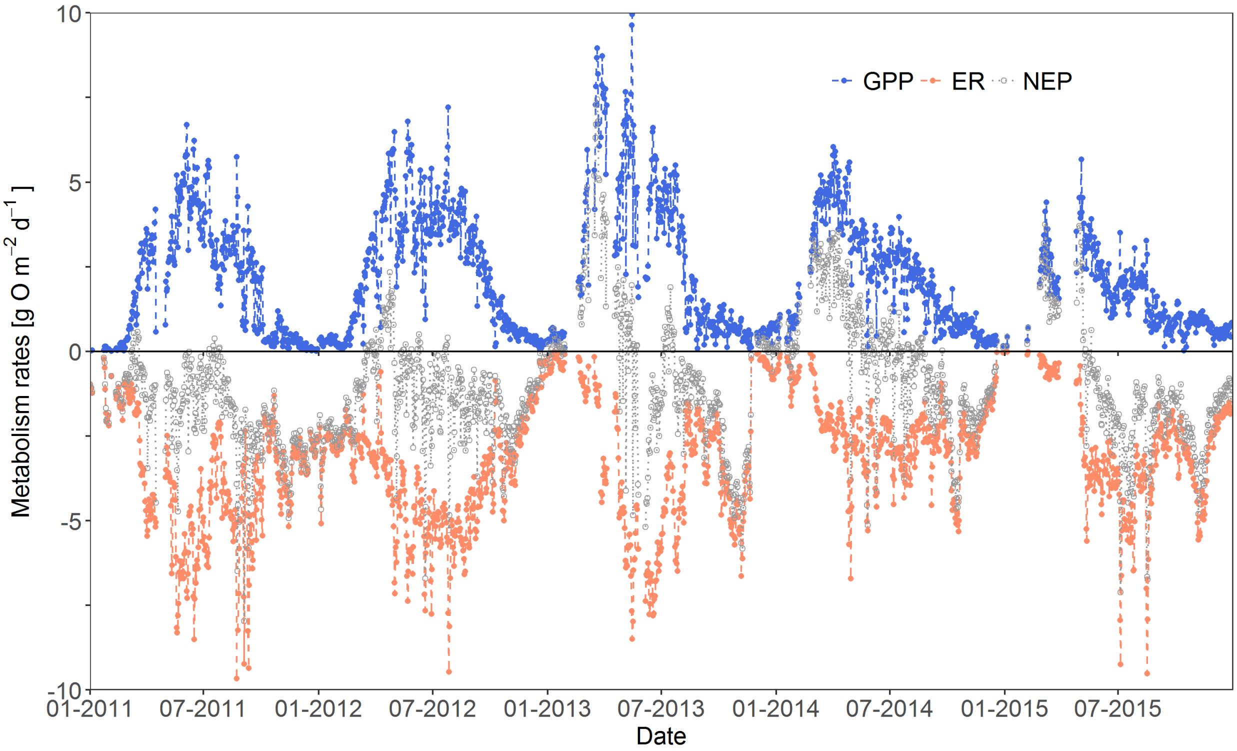
GPP
ER
NEP
Metabolism rates [g O m^{-2} d^{-1}]
10
5
0
-5
-10
01-2011
07-2011
01-2012
07-2012
01-2013
07-2013
01-2014
07-2014
01-2015
07-2015
Date

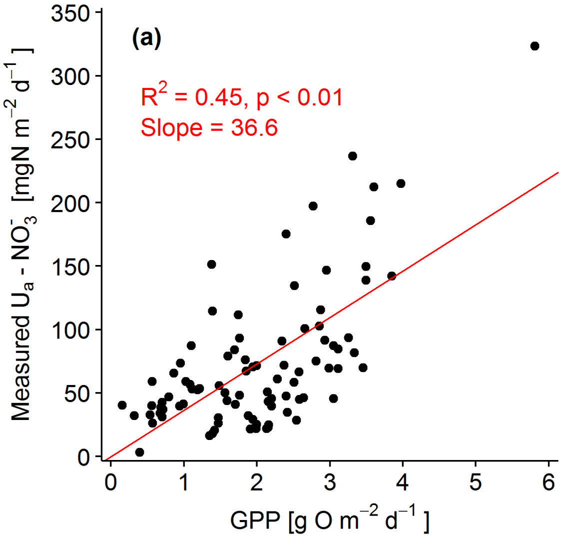
(a)
$R^2 = 0.45, p < 0.01$
Slope = 36.6
Measured U_a - NO_3^- [mgN m^{-2} d^{-1}]
0
50
100
150
200
250
300
350
0
1
2
3
4
5
6
GPP [g O m^{-2} d^{-1}]

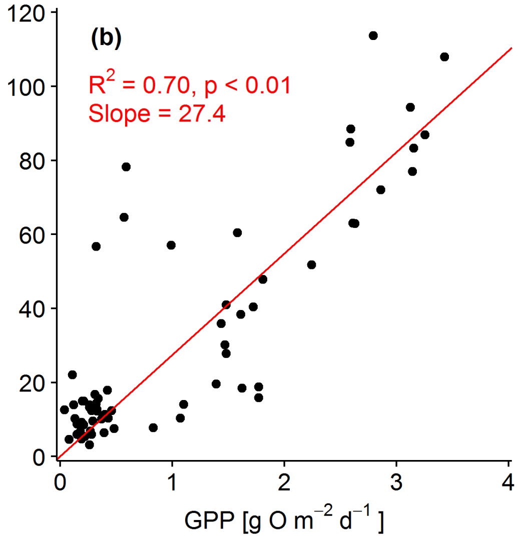
(b)
$R^2 = 0.70, p < 0.01$
Slope = 27.4
0
20
40
60
80
100
120
0
1
2
3
4
GPP [g O m^{-2} d^{-1}]

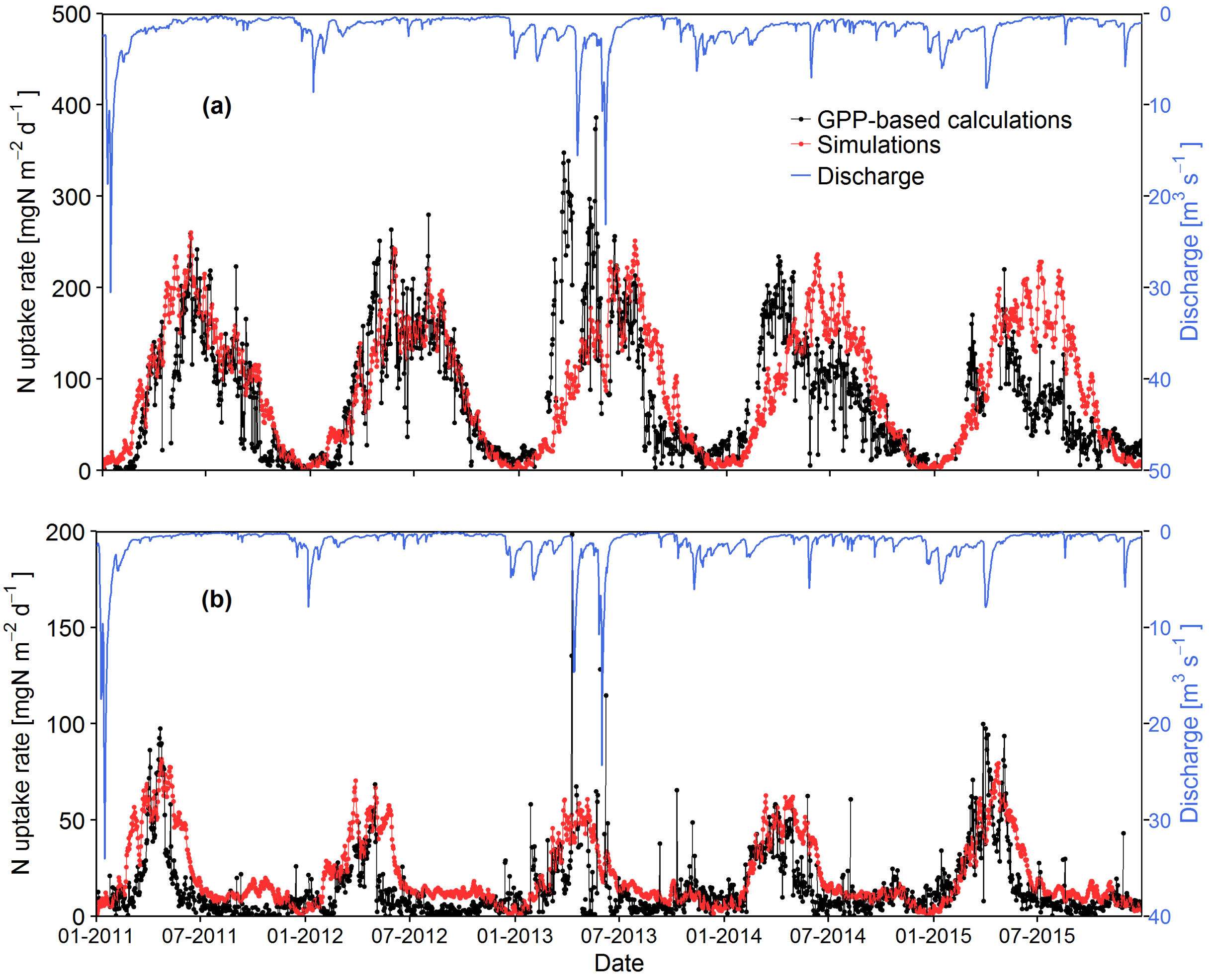
(a)
(b)
GPP-based calculations
Simulations
Discharge
N uptake rate [mgN m^{-2} d^{-1}]
Discharge [m^3 s^{-1}]
500
400
300
200
100
0
150
50
-10
-20
-30
-40
-50
01-2011
07-2011
01-2012
07-2012
01-2013
07-2013
01-2014
07-2014
01-2015
07-2015
Date

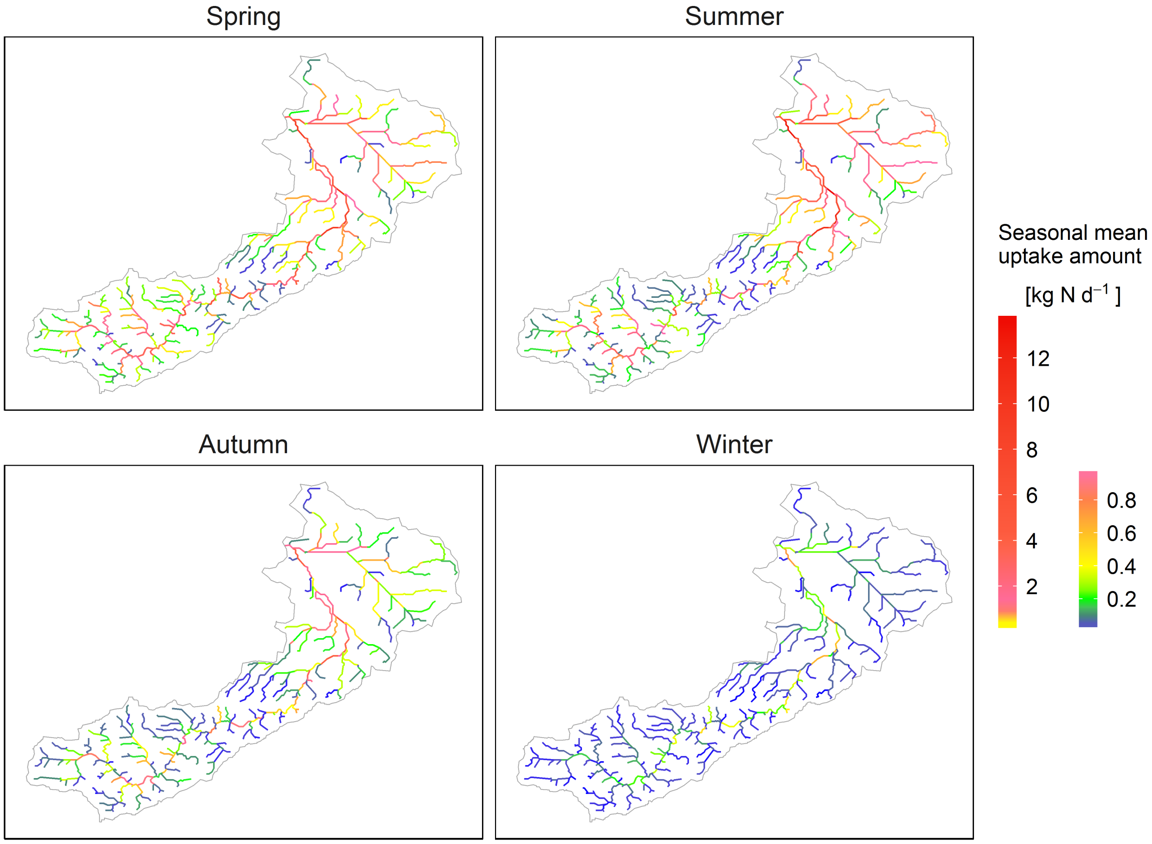
Spring
Summer
Autumn
Winter
Seasonal mean uptake amount
[kg N d^{-1}]
12
10
8
6
4
2
0.8
0.6
0.4
0.2

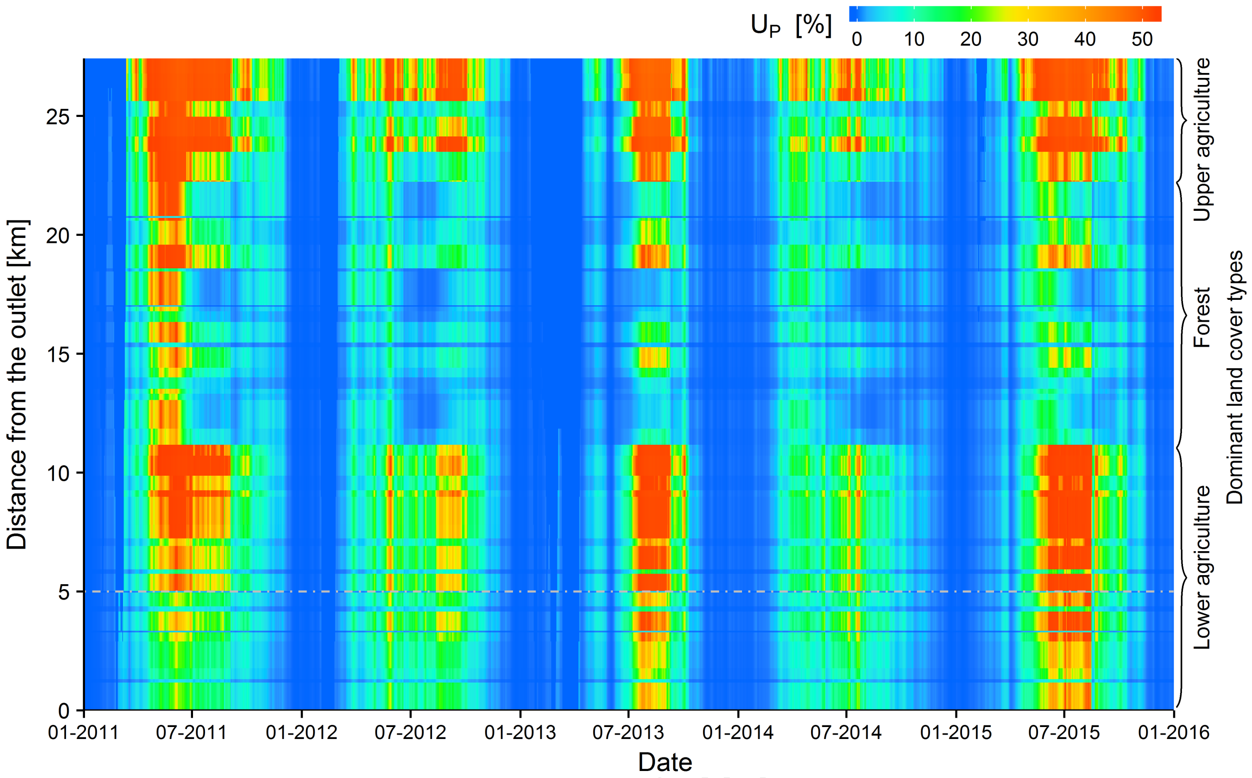
U_P [%]
0
10
20
30
40
50
Distance from the outlet [km]
0
5
10
15
20
25
01-2011
07-2011
01-2012
07-2012
01-2013
07-2013
01-2014
07-2014
01-2015
07-2015
01-2016
Date
Upper agriculture
Forest
Lower agriculture
Dominant land cover types

Highlights:

- Stream metabolism differs significantly under different riparian conditions
- Continuous $U_{a-NO_3^-}$ can newly be obtained based on its robust correlation with GPP
- A parsimonious approach for regionalizing $U_{a-NO_3^-}$ is validated using the new data
- Networked upscale modeling reveals high spatiotemporal variability of nitrate uptake
- Uptake efficiency varies depending on riparian shading and hydrochemical conditions

We declare no conflict of interest.